

# Flapping States of a Flag in an Inviscid Fluid: Bistability and the Transition to Chaos

Silas Alben\*

*School of Mathematics, Georgia Institute of Technology, Atlanta, Georgia 30332-0160, USA*

Michael J. Shelley

*Applied Math Laboratory, Courant Institute, New York University, New York, New York 10012, USA*

(Received 26 October 2007; published 21 February 2008)

We investigate the “flapping flag” instability through a model for an inextensible flexible sheet in an inviscid 2D flow with a free vortex sheet. We solve the fully-nonlinear dynamics numerically and find a transition from a power spectrum dominated by discrete frequencies to an apparently continuous spectrum of frequencies. We compute the linear stability domain which agrees with previous approximate models in scaling but differs by large multiplicative factors. We also find hysteresis, in agreement with previous experiments.

DOI: [10.1103/PhysRevLett.100.074301](https://doi.org/10.1103/PhysRevLett.100.074301)

PACS numbers: 46.40.Jj, 46.40.Ff, 47.15.ki, 47.52.+j

A longstanding problem in the coupled motion of elastic bodies and high-speed flows is the instability underlying the flapping of flags. One of the earliest attempted explanations dates to Lord Rayleigh, who made an analogy to an instability of a fluid jet [1]. Since the 1930s, workers in aeronautics and applied mechanics have addressed the stability problem using linearized and approximate flow models [2–4], and empirical models [5]. Recent models [6–8] have recalled some elements of this earlier work while introducing new approximations. Realistic unsteady flow solvers allow for numerical simulations at moderate Reynolds numbers ( $O(10^2)$ ) [9,10] but accurate studies at higher Reynolds numbers are difficult due to the necessity to resolve the production and dynamics of thin free shear layers.

In this work we simulate the nonlinear dynamics of a heavy elastic sheet which moves in a 2D inviscid fluid and sheds a vortex sheet from its trailing edge. Most previous flag models can be considered as approximations, with varying degrees of accuracy, to this model. We characterize the behavior of flapping flags at large amplitudes and over many flapping periods, and demonstrate a transition from periodic to chaotic flapping as bending rigidity is decreased. We also determine the stability boundary of the flow-aligned state for the flag, in the two-dimensional parameter space of dimensionless flag inertia and bending rigidity, and compare this with two recent models [7,8]. This comparison indicates that greatly-simplified models coupling flag rigidity, and flag and fluid inertia, can yield a qualitative understanding of flag stability. Finally, we demonstrate that this model exhibits bistability over a range of dimensionless rigidity, which is consistent with recent experiments of Zhang *et al.* in soap-film flows [11] and of Shelley *et al.* in water tunnels [8].

*The flag model.*—We consider the 2D flag as an inextensible elastic sheet of length  $L$ , mass per unit length  $\rho_s$ , and rigidity  $B$ , moving under the pressure forces of a surrounding inviscid and incompressible fluid of density

$\rho_f$  (here, mass per unit area) that moves past the flag with free-stream speed  $U$ . Scaling space on  $L$ , and time on  $L/U$ , the flag with position  $\mathbf{X}(s, t)$  ( $s$  is arclength;  $0 \leq s \leq 1$ ) evolves via Newton’s 2nd law as

$$R_1 \mathbf{X}_{tt} = \partial_s(T\hat{\mathbf{s}}) - R_2 \partial_{ss}(\kappa\hat{\mathbf{n}}) - [p]\hat{\mathbf{n}}, \quad (1)$$

where  $T$  is the tension that enforces inextensibility,  $[p]$  is the pressure jump across the flag, and  $\kappa$  is the flag curvature. The tension has been scaled by  $\rho_f U^2 L$ , the pressure by  $\rho_f U^2$ , and  $R_1$  and  $R_2$  are the two control parameters of the dynamical system with  $R_1 = \rho_s/\rho_f L$  the dimensionless mass of the flag and  $R_2 = B/\rho_f U^2 L^3$  its dimensionless rigidity (also an inverse square velocity). The sheet is held and clamped at  $s = 0$ , its leading end, with zero deflection. Free-end boundary conditions are assumed at  $s = 1$  with  $T = \kappa = \kappa_s = 0$  there, and the tension can be eliminated from Eq. (1) by integration of the  $\hat{\mathbf{s}}$  component from  $s = 1$ .

As the flag is also a surface in the flow, by the kinematic boundary condition it must move with normal velocity  $\nu$  of the fluid, which is continuous across  $C_b$  although the tangential velocity is not. Hence we can write

$$\mathbf{X}_t = \nu\hat{\mathbf{n}} + \tau\hat{\mathbf{s}}, \quad (2)$$

where the choice  $\tau = \int_0^s ds' \nu(s') \kappa(s')$  enforces the same frame as is implicit in Eq. (1), i.e.,  $s$  is independent of  $t$ . The wake shed behind the flag is modeled as a (free) vortex sheet (labeled  $C_f$  in Fig. 1), or a  $\delta$ -function distribution of vorticity along a curve in the plane. The flag can also be considered a (bound) vortex sheet (labeled  $C_b$  in Fig. 1) due to the tangential velocity jump across it. The velocity induced by the singular vorticity distribution on  $C = C_b + C_f$  is given by the Biot-Savart integral, and relative to the background flow is:

$$\mathbf{u}(\mathbf{x}) = \hat{\mathbf{x}} + \frac{1}{2\pi} \int_C ds' \gamma(s') \frac{(\mathbf{x} - \mathbf{X}(s'))^\perp}{|\mathbf{x} - \mathbf{X}(s')|^2}, \quad (3)$$

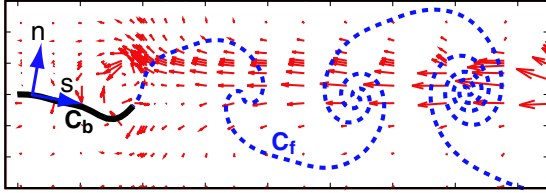


FIG. 1 (color online). Flag and wake dynamics for  $R_1 = 0.3$  and  $R_2 = 0.01445$ . The time-averaged flow velocity field of the flag from  $t = 0$  to  $t = 120$  is shown (red arrows: average over 60 flapping periods), with the background velocity removed. The flag position ( $C_b$ , in black, with normal  $\hat{\mathbf{n}}$  and tangent  $\hat{\mathbf{s}}$  labeled) and trailing vortical wake (the free-sheet  $C_f$ , blue-dashed line) is shown at  $t = 120$ .

where  $\mathbf{x}^\perp = (-y, x)$ ,  $\gamma$  is the vortex sheet strength (the jump in tangential velocity across the sheet), and  $\mathbf{u}$  satisfies the condition of zero jump in normal velocity. The average of velocities above and below  $C$  is

$$\mathbf{W}(s) = \hat{\mathbf{x}} + \frac{1}{2\pi} \oint_C ds' \gamma(s') \frac{(\mathbf{X}(s) - \mathbf{X}(s'))^\perp}{|\mathbf{X}(s) - \mathbf{X}(s')|^2}, \quad (4)$$

where the Birkhoff-Rott integral is of principal value type. Hence,  $\nu = \mathbf{W} \cdot \hat{\mathbf{n}}$ . The evolution of  $\gamma$  on  $C_b$  is determined by taking the tangential component of the difference of limits of the Euler equations above and below the flag (expressed in the frame where  $s$  is independent of  $t$ ), yielding

$$\gamma_t + \partial_s[(\mu - \tau)\gamma] = \partial_s[p], \quad (5)$$

where  $\mu = \mathbf{W} \cdot \hat{\mathbf{s}}$ . Using that  $[p]_{s=1} = 0$ , Eq. (5) can be integrated across  $C_b$  to eliminate  $[p]$ . On  $C_f$ ,  $[p] = 0$  and the evolution of  $\gamma$  is best considered in the average velocity frame where  $\gamma_t = 0$ , and hence is invariant. A convenient parametrization of  $C_f$  is then total circulation  $\Gamma_0$  to the free end of the flag with its initial value determined by the shedding condition from the flag end  $\dot{\Gamma}_0 = \gamma\nu|_{s=1}$  (see Jones [12]). We omit the small leading-edge vortex, which gives a small perturbation to the transverse pressure forces which drive the flag. We also neglect shear stresses in this simple model, which are dominated by pressure forces when the flag undergoes  $O(1)$  deflections, but may nonetheless be important for determining the onset of flapping.

*The numerical method.*—We evolve Eqs. (1), (2), and (5), and boundary conditions, numerically by expanding  $\mathbf{X}$ ,  $[p]$ , and  $\gamma$  on the flag as first-kind Chebyshev polynomials. This representation is convenient for evaluating the integral in Eq. (4) [13]. The system is discretized to second-order implicitly in time (for stability purposes) with new segments of the free vortex sheet created at each time step [12]. The set of nonlinear discrete Eqs. (1), (2), and (5) is solved by a Newton iteration.

At each time step, after convergence of the Newton iteration, Eq. (4) is used to update the position of the free sheet. On the free sheet, the singular kernel  $\mathbf{x}^\perp/|\mathbf{x}|^2$  is mollified and replaced by the smoothed kernel  $\mathbf{x}^\perp/(|\mathbf{x}|^2 +$

$\delta^2$ ), as used by Krasny [14] and many others since. This allows vorticity accumulations along the free sheet to form vortical spirals [14]. Here we set  $\delta$  equal to 0.2, small enough to capture well-defined vortical rolls in the wake. On the bound sheet (the flag) we retain the singular kernel, as mollifying there makes the matrix underlying the Newton iteration ill-conditioned.

The code shows convergence at the expected orders as the spatial and temporal grids are refined. We have reproduced known steady flows past rigid plates [15]. We have also compared an impulsively started flat plate, for which a growth rate of circulation of  $\Gamma_0 \sim t^{1/3}$  is predicted [12,16]. We find a temporal exponent of  $0.34 \pm 0.02$  between  $t = 0$  and 1, for  $\delta = 0.1$  and 0.2, which is the same growth reported by Jones for  $\delta = 0.2$  [12].

*Results.*—We first demonstrate that our flag model captures phenomena previously observed in experiment (e.g., [8,11]). Figure 1 (and supplementary materials [17]) shows the result of a long-time simulation using  $R_1 = 0.3$  and  $R_2 = 0.01445$ , values for which only steady flapping with a well-defined period is observed over a broad range of initial perturbations. Here, the dynamics was induced by smoothly perturbing the leading-edge position [of amplitude  $O(10^{-5})$ ], while smoothly ramping the background flow velocity up to unity. By  $t \approx 10$ , exponential growth of the initial perturbation has saturated, and the flag has entered a periodic flapping state, shown in Fig. 1 at  $t = 120$ . The trailing shed sheet has rolled up into spiral vortices associated with local Kelvin-Helmholtz instabilities [15], and has formed a “von Kármán” vortex street (see also the supplementary movies [17]). The time-averaged velocity field with the background flow removed is directed upstream towards the flag. The upstream fluid momentum thus generated is associated with a drag force on the flag.

A sequence of snapshots for this case is shown in Fig. 2(a), in which a simple periodic flapping dynamics is seen. The flapping consists of backwards traveling waves of simple spatial form, with a wave envelope that is roughly linear in distance from the flag support point. The temporal Fourier transform  $\hat{U}_\omega$  of the bending energy  $U = \int_{C_b} \kappa^2 ds/2$  is shown in Fig. 3(a). It is dominated by peaks at two distinct frequencies, the higher of which is a harmonic of the lower, and also has a small long-time component near frequency 0.4.

For a range of larger  $R_2$ , these frequencies change smoothly and reflect simple harmonic flapping. However, Fig. 3(b) shows the temporal spectrum from a long-time simulation from the same initial conditions if  $R_2$  is very slightly decreased (to  $R_2 = 0.01436$ ,  $\sim 1\%$  change). The dominant frequencies shift abruptly higher and new frequency components appear. This is associated with a change in flapping dynamics, illustrated by Figs. 2(b) and 3(c), for which  $R_2 = 0.0138$  [17]. In Fig. 2(b) the vortex wake is compressed relative to that in Fig. 2(a), due to the higher dominant frequency over which vorticity changes

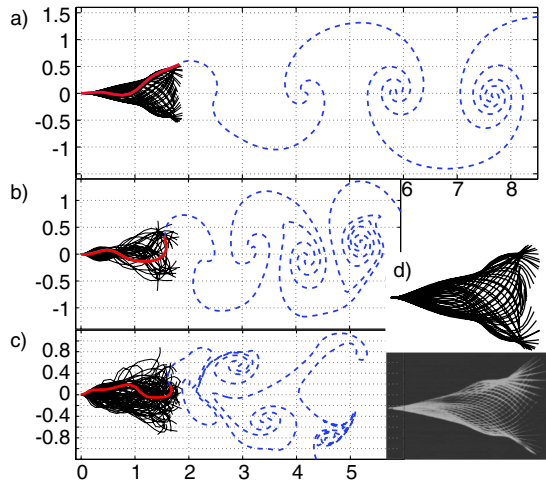


FIG. 2 (color online). Snapshots of the flag for fixed mass ( $R_1 = 0.3$ ) and decreasing rigidities  $R_2$ . (a) The observed flapping mode at  $R_2 = 0.01445$ , about a factor of 2 below the critical  $R_2 = 0.0262$ ; (b) a higher energy flapping mode for  $R_2 = 0.0138$ ; (c) a chaotic flapping mode at  $R_2 = 0.0025$ . (d) Comparison of experimental flag snapshots in [18], Fig. 12b, with model shapes. In both cases  $R_1 = 0.37$  (see text for  $R_2$ ).

sign. The fluid drag on the flag also increases dramatically with this transition from harmonic flapping, moving in time-average from 0.139 to 0.525 between panels *a* to *b*, with the drag time-trace punctuated by intermittent high-drag “flag-snapping” events (as is somewhat evident from Fig. 2(b)). In short, the sheet dynamics now has more degrees of freedom in both time and space, the latter being of larger amplitude and bending energy.

Further decreases in  $R_2$  introduce yet more spatial complexity as well as the broad spectral content characteristic

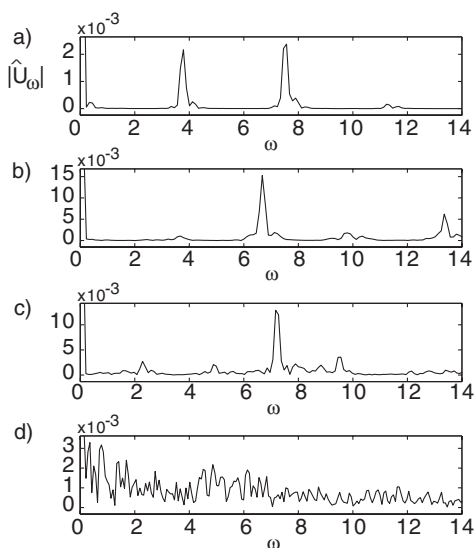


FIG. 3. Temporal power spectra of flag bending energy vs. frequency, for  $R_1 = 0.3$  and  $R_2$  equal to 0.01445 (a), 0.01436 (b), 0.0138 (c), and 0.0025 (d).

of chaotic dynamics. This is illustrated in Figs. 2(c) and 3(d) [17] for which  $R_2 = 0.0025$ . The flag snapshots over regular time intervals fill space within a roughly linear envelope, and the flag shape has become more irregular. The vortex wake seen in Fig. 2(c) retains predominantly single-signed vorticity above and below the center line, but the structure of the vortices and the spacing between them is irregular. The spectrum now shows no apparent dominant frequencies but rather a wide range of excited frequencies. Here the time-averaged fluid drag is 0.427, still large but somewhat decreased from the previous case.

As a point of comparison, in Fig. 2(d) we show snapshots from the model and from a recent experiment using a paper flag in air [18]. In both cases  $R_1 = 0.37$ . For the experiment,  $R_2$  is unavailable. For the model we take  $R_2 = 0.018$ , giving the longest wavelength mode; the snapshots vary little with  $R_2$  until the abrupt onset of a higher wavelength mode. The model shapes show larger curvatures but similar flapping amplitude (the model gives more similar shapes using  $R_1 = 0.25$ ). Possible reasons for the differences are 3D effects and skin friction in the experiment, and nonuniformity in the experimental flow.

*Linear stability.*—Here we study directly the linear stability of the straight flag, and assess recent models of the transition to instability. We infer stability directly by imposing small initial perturbations and tracking their growth (if any) in the full numerical system. By searching over a large portion of the  $R_1$ - $R_2$  space, we identified a boundary curve, plotted in Fig. 4, below which (in  $R_2$ ) small perturbations grow exponentially, with a rate which increases with distance from the line, and above which

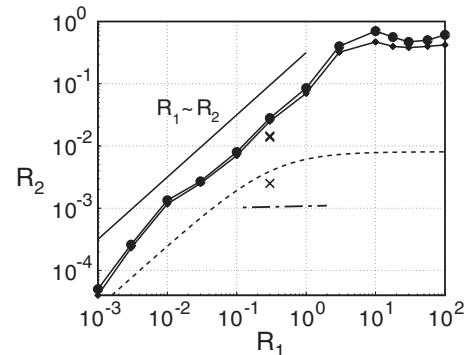


FIG. 4. Computed stability boundary in the  $R_1 R_2$  plane. The upper solid boundary gives the smallest  $R_2$  above which a small leading-edge forcing ( $y(t) = 10^{-5}(2t)^2 e^{-(2t)^2}$ ) does not lead to flapping. The lower solid boundary is the largest  $R_2$  below which such forcing leads to exponential growth of elastic energy in time until the flag saturates with  $O(1)$  flapping, as shown in Figs. 1 and 2. The solid line gives the scaling  $R_1 \sim R_2$  for small flag masses. The black crosses mark the cases shown in Fig. 2 [upper cross is (a) and (b), and lower is (c)]. The dashed line shows the stability boundary from [8], and the dash-dotted line the corresponding boundary plotted in Fig. 3 of [7] (showing only the portion  $R_2 \approx \text{const}$ , but having the same asymptotic scalings as the model here and in [8]).

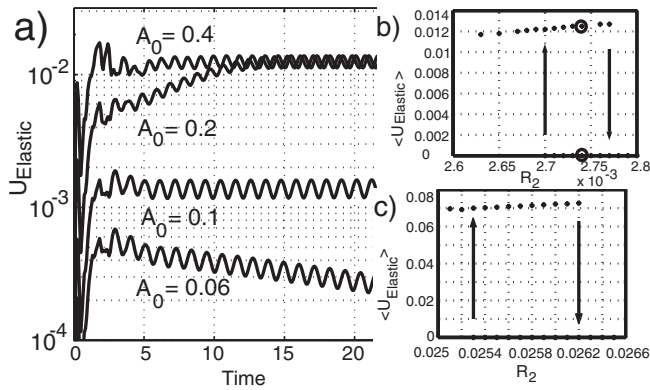


FIG. 5. Bistability and hysteresis in the onset of flapping with changes of flag rigidity  $R_2$ . (a) For  $R_1 = 0.03$  and  $R_2 = 2.74 \times 10^{-3}$ , four different values of transverse perturbations  $A_0(2t)^2 e^{-(2t)^2}$  are applied to the flag leading edge, for  $A_0$  in the range 0.06 to 0.4, and bending energy is plotted in time. The hysteresis loop for  $R_1 = 0.03$  is shown in (b), with the flat and steady flapping states in (a) circled. The time-averaged bending energy in the asymptotic steady state is plotted. (c) The hysteresis loop for mass  $R_1 = 0.3$ , an order of magnitude larger than in (b), showing a range of bistability which is also an order of magnitude larger.

perturbations in  $y$  do not increase. This stability boundary shows a linear slope at small  $R_1$ , where a proportionately small bending rigidity is needed for the instability to occur. At larger  $R_1$  the curve becomes nearly flat. A physical interpretation for the transition to instability is that greater flag inertia allows small oscillations of the flag to increase more readily against the damping of fluid inertia. Also plotted in Fig. 4 is the stability boundary (dashed line) for a biinfinite flag from [8]. It has the same asymptotic scalings but differs by a large multiplicative factor. This discrepancy is not surprising because the pressure distribution in the current model is dominated by vortex shedding, a term absent in the infinite flag model. The stability boundary presented in Argentina & Mahadevan [7] for an inviscid flow with vortex shedding has the same asymptotic scalings, though again with a different multiplicative factor (see Fig. 4). Their model approximates the flow around the flexible flag as the steady potential flow past a hinged rigid plate, scaled by a variable flag velocity. All three models have similar asymptotic scalings, presumably because the dominant terms in the flag equation have the same scaling with physical parameters in the three models.

**Bistability.**—Our nonlinear flag model supports bistability of the straight and flapping states, as has been observed experimentally [8,11] and numerically [9]. To show this, the initial perturbation amplitude applied to the flag was varied in a range of  $R_2$  near the stability boundary. Figure 5(a) shows the elastic energy in time for four different initial vertical perturbations. A division between the two states occurs for amplitude 0.1: Above this value, the perturbed flag reaches a unique state of large-amplitude

flapping, while below the perturbation decays to the straight flag case. This decay, and hence the bistability, may be surprising given the conservative nature of the system. However, the flag is coupled to the fluid, and by this can be convectively stabilized; if the flag perturbation is sufficiently small, it is simply swept into the wake and moved downstream.

The hysteresis loop corresponding to this value of  $R_1 = 0.3$  is shown in Fig. 5(b) and that for  $R_1 = 0.03$  in Fig. 5(c). We find that the hysteresis loops extend over factors of 1.025 to 1.04 in  $R_2$  in the two cases, compared with a factor of 2 in the experiment of ([8], Fig. 4) where  $R_1 = 0.05$ , and a factor of 1.33 in [18] for  $0.1 < R_1 < 1$ . The larger hysteresis in the experiments may be due to the effects of fluid viscosity and structural damping.

We thank M. Jones and J. Zhang for useful discussions. We note that J. Zhang has recently made informal observations of a transition in flag flapping behavior in soap-film flows similar to that seen between Figs. 2(a) and 2(b). S. A. acknowledges support from an NSF Mathematical Sciences Grant. M.J.S. acknowledges support from the DOE (No. DE-FG02-88ER25053).

\*alben@math.gatech.edu

- [1] Lord Rayleigh, Proc. London Math. Soc. **s1-10**, 4 (1878).
- [2] T. Theodorsen, NACA, Technical Report No. 496, 1935.
- [3] T. von Kármán and J. M. Burgers, in *Aerodynamic Theory*, edited by W. Durand (Springer-Verlag, Berlin, 1935), Vol. 2, p. 346.
- [4] H. Glauert, *The Elements of Airfoil and Airscrew Theory* (Cambridge University Press, Cambridge, England, 1947).
- [5] R. L. Bisplinghoff and H. Ashley, *Principles of Aeroelasticity* (Dover, New York, 2002).
- [6] A. D. Fitt and M. P. Pope, J. Eng. Math. **40**, 227 (2001).
- [7] M. Argentina and L. Mahadevan, Proc. Natl. Acad. Sci. U.S.A. **102**, 1829 (2005).
- [8] M. Shelley, N. Vandenberghe, and J. Zhang, Phys. Rev. Lett. **94**, 094302 (2005).
- [9] L. Zhu and C. S. Peskin, J. Comput. Phys. **179**, 452 (2002).
- [10] B. Connell and D. Yue, J. Fluid Mech. **581**, 33 (2007).
- [11] J. Zhang, S. Childress, A. Libchaber, and M. Shelley, Nature (London) **408**, 835 (2000).
- [12] M. Jones, J. Fluid Mech. **496**, 405 (2003).
- [13] M. A. Golberg, *Numerical Solution of Integral Equations* (Plenum, New York, 1990).
- [14] R. Krasny, J. Comput. Phys. **65**, 292 (1986).
- [15] P. Saffman, *Vortex Dynamics* (Cambridge University Press, Cambridge, England, 1992).
- [16] D. I. Pullin, J. Fluid Mech. **88**, 401 (1978).
- [17] See EPAPS Document No. E-PRLTAO-100-038805 for four supplementary movies, showing the transition from single-frequency to chaotic flapping. For more information on EPAPS, see <http://www.aip.org/pubservs/epaps.html>.
- [18] Y. Watanabe, S. Suzuki, M. Sugihara, and Y. Sueoka, J. Fluids Struct. **16**, 529 (2002).